# Phase-field simulation of domain size effect on dielectric and piezoelectric responses in $K_{0.5}Na_{0.5}NbO_3 \ epitaxial \ thin \ films \ with \ superdomain \ structures$

Meng-Jun Zhou<sup>1,a,\*</sup>, Bo Wang<sup>2,4,a,\*</sup>, Kun Peng<sup>1</sup>, Han-Xing Liu<sup>1</sup>, Long-Qing Chen<sup>2</sup>, and Ce-Wen Nan<sup>3</sup>

<sup>1</sup>State Key Laboratory of Advanced Technology for Materials Synthesis and Processing,
Center of Smart Materials and Devices, School of Material Science and Engineering, Wuhan
University of Technology, Wuhan, 430070, China

<sup>2</sup>Department of Materials Science and Engineering and Materials Research Institute, The Pennsylvania State University, University Park, Pennsylvania 16802, USA

<sup>3</sup>School of Materials Science and Engineering, State Key Lab of New Ceramics and Fine Processing, Tsinghua University, Beijing, 100084, China

<sup>4</sup>Materials Science Division, Lawrence Livermore National Laboratory, Livermore, CA 94550, USA

<sup>&</sup>lt;sup>a</sup> These authors contributed equally to this work.

<sup>\*</sup> Corresponding authors

#### **Abstract**

Size effects of mesoscale ferroelectric domains on the macroscopic dielectric and piezoelectric responses in domain-engineered bulk piezocrystals have been extensively studied for more than two decades. However, less is known about the domain size effects in ferroelectric epitaxial thin films, especially for films consisting of low-symmetry ferroelectric phases and exhibits hierarchical superdomain structures. Herein, using phase-field simulations, we systemically evaluate the effective out-of-plane dielectric and piezoelectric coefficients,  $\kappa_{33}^*$  and  $d_{33}^*$ , as a function of the domain periods for two types of superdomain structures in ferroelectric  $K_{0.5}Na_{0.5}NbO_3$  epitaxial thin films. In one type of the superdomain structures, we find that more than 70% increase of  $\kappa_{33}^*$  and nearly 20% increase of  $d_{33}^*$  can be achieved by tuning the domain period by a few tens of nanometers. Dissimilar behaviors are found when the domain period varies along different lateral directions, suggesting anisotropic domain size effects in thin films. By analyzing the local dielectric and piezoelectric responses from each domain variants and domain walls, we reveal that the domain size effect is governed by the variation of out-of-plane polarization inside the domains. Moreover, we also demonstrate enhanced domain size effects by modulating the misfit strains and temperature to approach the polymorphic phase boundaries, suggesting tunability of the size effect by doping and strain engineering. Our results reveal multimodal domain size dependence of dielectric and piezoelectric responses in low-symmetry ferroelectric epitaxial thin films, implying that domain size engineering can be used to tune macroscopic properties of thin-film ferroelectrics, similar to their bulk counterparts.

**Keywords:** ferroelectric thin film, domain structure, piezoelectric properties, dielectric properties, phase-field simulation,  $K_{0.5}Na_{0.5}NbO_3$ 

#### 1. Introduction

Piezoelectricity refers to the capability of materials to convert between mechanical and electrical energies in terms of stress-induced electrical current and electric field-induced displacement. As a result, piezoelectric materials underpin a variety of electromechanical applications such as sensors, actuators, and ultrasound transducers[1]. The most widely used family of high-performance piezoelectric materials is the perovskite ferroelectric oxides, including lead zirconate titanate, barium titanate BaTiO<sub>3</sub>, and relaxor-PbTiO<sub>3</sub>-based solid solutions, in the form of ceramics, bulk single crystals and thin films[2]. Recent advances in the study of piezoelectric materials aim at developing more advanced materials with higher piezoelectric coefficients [3,4] as well as looking for nontoxic alternative materials with comparable performance as the prevailing lead-containing ones [5].

The progress made in the development of high-performance materials is benefited from the fundamental understanding of the origin of piezoelectric responses. Generally, the piezoelectric responses of materials originate from intrinsic and extrinsic contributions[6,7]. The intrinsic piezoelectric response refers to the field-induced lattice distortion associated with the change of the polarization, including polarization extension and rotation which depends on the field direction with respect to the electric dipole orientation[8]. Extrinsic contributions may come from many distinct mechanisms, such as domain walls displacement [7], breaking of centrosymmetry (i.e., flexoelectric effect [9] or compositional gradients [10]), field-induced phase transitions [11], presence of antiphase boundaries [12], domain wall-dislocation interactions [13,14] and migration of charged point defects[15]. The extrinsic contributions may dominate the intrinsic ones in some cases and give rise to giant piezoelectricity even in

centrosymmetric materials[15].

It has been known for long that the mesoscale microstructures of materials have a strong influence on its piezoelectric properties [16,17]. For example, the piezoelectric responses of polycrystalline BTO ceramics depend on the grain size [18], and higher piezoelectric responses are found in ceramics with finer grains, which was attributed to the increase of the density of mobile domain walls. The piezoelectric response of single crystals strongly depends on its orientation. For many perovskite ferroelectrics, the largest longitudinal piezoelectricity is found when the crystal is poled along a nonpolar direction wherein more than one symmetryequivalent domain variants coexist and is known as the domain-engineered piezocrystals. It has also been found that the piezoelectric properties of the domain-engineered crystals vary with the average size of the domains. Although many earlier works reported that smaller domains lead to higher piezoelectricity [19-26], recent experimental and theoretical studies have revealed that the domain size effect on piezoelectricity can be more complex than expected. For example, opposite domain size effect wherein large domain yields higher piezoelectric properties has been revealed in relaxor-PbTiO<sub>3</sub> single crystals [3]. Moreover, it has been theoretically predicted that non-monotonous domain size dependence can appear in specific domain structures[27].

For piezoelectric effects in ferroelectric thin films, many studies have been focusing on the influences of film thickness and misfit strains on the piezoelectric responses [28,29]. It has been well-established that the clamping effect from the substrate can change the intrinsic piezoelectricity [30,31] by modifying the free energy landscape of the crystal and the extrinsic contribution by restricting the domain wall motion [32,33]. Therefore, the domain wall motion in thin films is largely restricted comparing with their bulk counterparts. In contrast, much less is known about the domain size effect on piezoelectric properties in ferroelectric thin films. Is there any significant domain size dependence of piezoelectricity in thin films? If yes, do smaller or larger domains give rise to higher piezoelectricity? What is the mechanism of the domain size dependence in epitaxial thin films? Can the domain size effect be modulated? As piezoelectric thin films are key active components for applications such as nano-/micro-electromechanical systems[34], answers to these questions are of both fundamental scientific interest and technical relevance.

Here, we aim to address the above questions by theoretically evaluating the domain size effect on the out-of-plane piezoelectric response in ferroelectric epitaxial thin films using phase-field simulations. We choose the K<sub>0.5</sub>Na<sub>0.5</sub>NbO<sub>3</sub> (KNN) epitaxial thin film as a model system which have aroused increasing research interests in recent years due to its lead-free nature, high piezoelectric activity[35–37], and capability of forming a rich variety of periodic and regular domain structures [38].

# 2. Phase-field modeling of superdomain structures and calculation of effective piezoelectric coefficient

We performed phase-field simulations using the ferroelectrics module of the phase-field package  $\mu$ -Pro<sup>®</sup>. The total free energy F of the thin film system consists of contributions from bulk energy  $f_{\text{bulk}}$ , gradient energy  $f_{\text{grad}}$ , electric energy  $f_{\text{elec}}$ , elastic energy  $f_{\text{elas}}[39-41]$ , i.e.,

$$F = \int_{V} [f_{\text{bulk}}(P_i) + f_{\text{grad}}(P_{i,j}) + f_{\text{elec}}(P_i, E_i) + f_{\text{elas}}(P_i, \varepsilon_{ij})] dV$$
 (1)

where  $P = (P_1, P_2, P_3)$  is the spontaneous polarization,  $E_i$  is the electric field,  $\varepsilon_{ij}$  is the total

strain, and V is the system volume. The detailed formulations for  $f_{\text{bulk}}$ ,  $f_{\text{grad}}$ ,  $f_{\text{elec}}$  and  $f_{\text{elas}}$  are given below. For KNN thin film, an  $8^{\text{th}}$ -order polynomial is used for the bulk energy  $f_{\text{bulk}}$ , i.e.,

$$\begin{split} f_{\text{bulk}} &= \alpha_1 (P_1^2 + P_2^2 + P_3^2) + \alpha_{11} (P_1^4 + P_2^4 + P_3^4) + \alpha_{12} (P_1^2 P_2^2 + P_1^2 P_3^2 + P_2^2 P_3^2) \\ &+ \alpha_{111} (P_1^6 + P_2^6 + P_3^6) + \alpha_{112} [(P_1^2 + P_2^2) P_3^2 + (P_1^2 + P_3^2) P_2^2 + (P_2^2 + P_3^2) P_1^2)] \\ &+ \alpha_{123} P_1^2 P_2^2 P_3^2 + \alpha_{1111} (P_1^8 + P_2^8 + P_3^8) + \alpha_{1122} (P_1^4 P_2^4 + P_1^4 P_3^4 + P_2^4 P_3^4) \\ &+ \alpha_{1112} [(P_1^2 + P_2^2) P_3^6 + (P_1^2 + P_3^2) P_2^6 + (P_2^2 + P_3^2) P_1^6)] \\ &+ \alpha_{1123} (P_1^4 P_2^2 P_3^2 + P_1^2 P_2^4 P_3^2 + P_1^2 P_2^2 P_3^4) \end{split} , \tag{2}$$

where the  $\alpha$ 's are the Landau coefficients determined under the stress-free condition[31]. The gradient energy  $f_{\text{grad}}$  is written as

$$f_{\text{grad}} = \frac{1}{2} g_{11} (P_{1,1}^2 + P_{2,2}^2 + P_{3,3}^2) + g_{12} (P_{1,1} P_{2,2} + P_{1,1} P_{3,3} + P_{2,2} P_{3,3}) + + \frac{1}{2} g_{44} ((P_{1,2} + P_{2,1})^2 + (P_{1,3} + P_{3,1})^2 + (P_{2,3} + P_{3,2})^2)$$
(3)

where the  $g_{11}$ ,  $g_{12}$  and  $g_{44}$  represent the gradient energy coefficients, and  $P_{i,j} = \frac{\partial P_i}{\partial x_j}(i,j = 1,2,3)$ . The electric energy  $f_{\text{elec}}$  can be written as

$$f_{\text{elec}} = -\frac{1}{2} \kappa_0 \kappa_{ij}^b E_i E_j - E_i P_i, \qquad (4)$$

where the  $\kappa_0$ ,  $\kappa_{ij}^b$  and  $E_i$  in Eq. (4) are the vacuum dielectric permittivity, the background relative dielectric permittivity tensor and electric field, respectively. The elastic energy  $f_{\rm elas}$  can be written as

$$f_{\text{elas}} = \frac{1}{2} c_{ijkl} (\varepsilon_{ij} - \varepsilon_{ij}^{0}) (\varepsilon_{kl} - \varepsilon_{kl}^{0}), \qquad (5)$$

where the  $c_{ijkl}$ ,  $\varepsilon_{ij}$ ,  $\varepsilon_{ij}^0$  represents the elastic stiffness tensor, total strain, and eigenstrain. The eigenstrain is related to the spontaneous polarization through the electrostrictive effect,  $\varepsilon_{ij}^0 = Q_{ijkl}P_kP_l$ , where  $Q_{ijkl}$  is the electrostrictive tensor. All the coefficients adopted in Eq.(2-5) for KNN can be found in literatures[31,38,42,43].

The evolution of P is governed by the time-dependent Ginzburg-Landau (TDGL)

equation,

$$\frac{\partial P_i(x,t)}{\partial t} = -L \frac{\delta F}{\delta P_i(x,t)}, \quad (i = 1, 2, 3)$$
 (6)

with L representing the kinetic coefficient. At each time step, the electrostatic and mechanical equilibrium equations are solved simultaneously with the short-circuit electric boundary conditions and mixed-typed mechanical boundary conditions, respectively[39,41]. The simulation system is discretized into  $128\Delta x \times 128\Delta y \times 36\Delta z$  grid points with the grid size  $\Delta x = \Delta y = \Delta z = 1$  nm. In all simulations of this work, the thickness of the KNN thin film is taken to be 20 nm, and the thickness of substrate layer is taken to be 13 nm. Notably, the substrate thickness in reality is usually much larger than the film. The value 13 nm is chosen here based on the assumption that the elastic deformation into the substrate can be ignored beyond this threshold. Detailed discussion on the choice of the substrate layer thickness can be found in Ref. [39].

To evaluate the domain size dependence of dielectric and piezoelectric responses, we first obtained the equilibrium domain structures of the  $a_1a_2/ac$ -type and  $a_1c/a_2c$ -type superdomains in KNN thin film by relaxing the preset domain structure with a prescribed domain period under zero macroscopic electric fields and stress. To obtain a superdomain structure with well-defined domain size, we preset the initial polarization configuration of the system by assigning local polarization vectors with corresponding directions (e.g., P//[110] for  $a_1^+a_2^+$  domain) and a uniform small magnitude (|P| = 0.1 C/m<sup>2</sup>). Then, these preset states were taken as the initial states to the simulations for relaxation. To avoid relaxing into different domain states and destroy the preset superdomain structure, we also turned off random noise during the relaxation

process. This method was used to obtain superdomain structures with regular morphology in our previous work [38]. In all cases studied here, there is no emergence of new domains or disappearance of preset domains during the relaxation, and hence the domain sizes of the preset structures are maintained.

Notably, in experiments, the piezoelectric coefficients are measured after poling the sample. To consider the poling process, only domain structures with net out-of-plane polarization are investigated in our work. Next, we applied a series of small electric fields  $E_3$  (lower than 0.2 MV/m) along the out-of-plane direction of the film and monitor the changes of out-of-plane polarization  $\Delta P_3$  and strain component  $\Delta \varepsilon_{33}$  of the films. The corresponding effective out-of-plane dielectric coefficient  $\kappa_{33}^*$  and converse piezoelectric coefficient  $d_{33}^*$  can be obtained by,

$$\kappa_{33}^* = \frac{1}{\kappa_0} \frac{\partial \Delta P_3}{\partial E_3} \quad , \tag{7}$$

and

$$d_{33}^* = \frac{\partial \Delta \varepsilon_{33}}{\partial E_3}.$$
 (8)

An example of calculating  $\kappa_{33}^*$  and  $d_{33}^*$  is given in Fig. S1. It can be seen that  $\Delta P_3$  and  $\Delta \varepsilon_{33}$  are both linear with respect to the applied electric filed  $E_3$ . Therefore,  $\kappa_{33}^*$  and  $d_{33}^*$  can be obtained by the slopes of the  $\Delta P_3$ - $E_3$  and  $\Delta \varepsilon_{33}$ - $E_3$  curves, respectively. Since the intrinsic dielectric and piezoelectric responses are considered in this work, the small magnitude of  $E_3$  ensures negligible contributions from domain wall motion or field-induced phase transitions. Note that the asterisk is used in the superscripts of  $\kappa_{33}^*$  and  $d_{33}^*$  to distinguish the effective properties along the out-of-plane direction of the  $(001)_{pc}$ -oriented film from the crystallographic  $\kappa_{33}$  and

 $d_{33}$  along the polar axis of a polar single domain. The subscript pc stands for the pseudocubic coordinates, which will be omitted in the following discussion unless otherwise mentioned.

#### 3. Results

#### 3.1 The $a_1a_2/ac$ -type and $a_1c/a_2c$ -type superdomain structures

For a bulk KNN single crystal at room temperature and ambient pressure, the orthorhombic phase (space group Amm2) is the thermodynamically stable state, which has twelve ferroelectric domain variants with spontaneous polarization along the <110> directions. However, for (001)-oriented KNN epitaxial thin film, the anisotropic misfit strains imposed by the substrate break the degeneracy of the ferroelastic domain variants, giving rise to monoclinic domains (space group Pm) with only in-plane polarization component ( $P_1 \neq 0$ ,  $P_2 \neq 0$ ,  $P_3 = 0$ ), denoted as  $a_1a_2$ , and domains with both in-plane and out-of-plane polarization components, denoted as  $a_1c$  ( $P_1 \neq 0$ ,  $P_2 = 0$ ,  $P_3 \neq 0$ ) and  $a_2c$  ( $P_1 = 0$ ,  $P_2 \neq 0$ ,  $P_3 \neq 0$ ). The  $a_1a_2$ -type domains include four variants depending on the sign of  $P_1$  and  $P_2$  denoted as  $a_1^+a_2^+$ ,  $a_1^-a_2^+$ ,  $a_1^+a_2^-$ , and  $a_1^-a_2^-$ . For example,  $a_1^-a_2^+$  domains have  $P_1 < 0$ ,  $P_2 > 0$ ,  $P_3 = 0$ . Likewise, the  $a_1c_1$ -type domains include  $a_1^+c_1^+$ ,  $a_1^-c_1^+$ ,  $a_1^+c_1^-$ ,  $a_1^-c_1^-$  domain variants and the  $a_2c_1$ -type domains include  $a_2^+c_1^+$ ,  $a_2^-c_1^+$ ,  $a_2^+c_1^-$ ,  $a_2^-c_1^-$  domain variants.

The spatial configurations of these three types of ferroelastic domains give rise to a variety of intriguing domain morphology in epitaxial  $K_xNa_{1-x}NbO_3$  thin films, some of which show hierarchical and regular patterns known as superdomains. For example, two typical superdomain structures have been reported in  $K_xNa_{1-x}NbO_3$  epitaxial thin films, namely, the  $a_1a_2/ac$ -type and  $a_1c/a_2c$ -type superdomains. The former type consists of a pair of polydomains of  $a_1a_2$  and ac ( $a_1c$  or  $a_2c$ ) domains while the latter is constituted by a pair of polydomains of

 $a_1c$  and  $a_2c$  domains. The  $a_1a_2/ac$ -type superdomains form in films under highly anisotropic misfit strains while the  $a_1c/a_2c$ -type is stabilized in films under moderate biaxial compressive misfit strains. Notably, there are many different variants for both types of superdomains consisting of different  $a_1a_2$  and ac domain variants [38]. However, only those superdomain structures with net out-of-plane polarization  $P_3$  have nonzero piezoelectric response, and thus will be the focus in this study. Without losing generality, we choose the  $a_1^+ a_2^+ / a_2^+ c^+ / / a_1^- a_2^+ /$  $a_2^+c^+$  as an example for the  $a_1a_2/a_2c$ -type superdomain and the  $a_1^-c^+/a_2^+c^+//a_1^+c^+/a_2^+c^+$  for the  $a_1c/a_2c$ -type superdomain, as shown in Fig. 1(a-b). Fig. 1(c-d) show the corresponding planar views of these two superdomain structures. Both types of superdomains show stripelike morphology but the stripes extend along different directions. Specifically, the stripes of the  $a_1c/a_2c$ -type superdomains extend along [110] and [1 $\bar{1}$ 0] while the stripes of the  $a_1a_2/a_2c$ -type superdomains are inclined by  $\sim \pm 20^{\circ}$  with respect to [010], which agree well with experimental measurements [44]. In addition, the  $a_1c/a_2c$ -type and  $a_1a_2/a_2c$ -type superdomains were termed as stripe-like and herringbone-like superdomains, respectively [45,46]. The definition of superdomain, superdomain wall, polydomain and domain walls are also illustrated in Fig.1 (e) for better understanding.

Following the procedure described in the Section 2, we evaluate the effective out-of-plane piezoelectric and dielectric coefficient,  $d_{33}^*$  and  $\kappa_{33}^*$ , as a function of the domain size for the two example superdomain structures. The domain size is defined by the lengths,  $L_x$  and  $L_y$ , representing the domain periods along the [100] and [010] directions, respectively, as labeled in Fig.1(c-d).

# 3.2 Domain size dependence of $d_{33}^*$ and $\kappa_{33}^*$ in $a_1a_2/a_2c$ -type superdomains

We start from the domain size effect on piezoelectric and dielectric properties in  $a_1a_2/a_2c$  superdomain structures. We artificially construct a series of  $a_1a_2/a_2c$  superdomain structures with different  $L_x$  (from 16 to 48 nm) and  $L_y$  (from 40 to 216 nm) and then relax the systems to equilibrium states under the anisotropic in-plane misfit strain of  $\varepsilon_{11}^{mis}$ = -0.4% and  $\varepsilon_{22}^{mis}$ = 1.0%. Fig. 2(a,c,e) show a few example superdomain structures obtained by this way with different  $L_x$  but fixed  $L_y$  (Fig. 2(a)), different  $L_y$  but fixed  $L_x$  (Fig. 2(c)), and varied  $L_y$  and  $L_x$  (Fig. 2(e)). The effective out-of-plane piezoelectric coefficient  $d_{33}^*$  and dielectric coefficient  $\kappa_{33}^*$  obtained by phase-field simulations as a function of  $L_x$  or  $L_y$  are shown in Fig. 2(b,d,f).

We find that when  $L_x$  is varied while keeping  $L_y = 128$  nm, both  $\kappa_{33}^*$  and  $d_{33}^*$  increase linearly with the domain size  $L_x$ . Approximately, 15% enhancement of  $d_{33}^*$  and more than 41% enhancement of  $\kappa_{33}^*$  can be achieved when  $L_x$  increases from 16 nm to 48 nm. When  $L_y$  is varied from 40 to 216 nm while keeping  $L_x = 32$  nm, both  $\kappa_{33}^*$  and  $d_{33}^*$  nonlinearly decrease with the increase of  $L_y$  with different extent (by 5% for  $d_{33}^*$  and 10% for  $\kappa_{33}^*$ ). The opposite trends when changing  $L_x$  or  $L_y$  suggest that the domain size effect in ferroelectric thin films can be anisotropic, i.e., distinct domain size dependence can be found when the domain changes size along different directions. Notably, the maximal  $\kappa_{33}^*$  along [001] achieved by domain size engineering can reach 780 within the calculated range, which is drastically higher than 233[42] of a single-domain orthorhombic-phase bulk KNN crystal, while the maximal  $d_{33}^*$  is 123 pC/N along [001], which is relatively lower than that of the bulk value 221 pC/N [47].

We also computed  $d_{33}^*$  and  $\kappa_{33}^*$  by simultaneously varying  $L_x$  and  $L_y$  with a fixed ratio of  $L_x/L_y = 1/4$ . Comparing with the cases in Fig. 2(b) and (d), the domain size effects become more complex when  $L_x$  and  $L_y$  vary simultaneously. The trends of  $d_{33}^*$  and  $\kappa_{33}^*$  are no longer

coincident: despite that  $\kappa_{33}^*$  increases monotonously with the domain size,  $d_{33}^*$  show a non-monotonous behavior. A dip of  $d_{33}^*$  is found at  $L_y = 80$  nm ( $L_x = 20$  nm) along with some fluctuations in the range  $60 < L_y < 100$  nm.

We further plotted all the calculated  $d_{33}^*$  and  $\kappa_{33}^*$  as a function of  $L_x$  and  $L_y$  in Fig. 3. It is found that  $d_{33}^*$  and  $\kappa_{33}^*$  show similar domain size dependence in general but with small deviations especially when  $L_y$  is small. Within the same range of domain sizes,  $\kappa_{33}^*$  show much higher tunability (from 511 to 874) than  $d_{33}^*$  (from 106 to 125 pC/N). Moreover, both materials responses depend more sensitively on  $L_x$  than  $L_y$ . Fig. 3 can be useful to guide the experimental optimization of dielectric and piezoelectric properties of KNN thin films by domain size engineering.

## 3.3 Domain size dependence of $d_{33}^*$ and $\kappa_{33}^*$ in $a_1c/a_2c$ superdomains

We then turn to assess the domain size effect on  $d_{33}^*$  and  $\kappa_{33}^*$  for  $a_1c/a_2c$ -type superdomains in KNN thin film. A series of  $a_1^+c^+/a_2^+c^+$  superdomains with different domain periods  $L_x$  and  $L_y$  under the in-plane misfit strain  $\varepsilon_{11}^{mis} = \varepsilon_{22}^{mis} = 0.075\%$  at 400 K are obtained as shown in Fig.4(a,c). Fig. 4(a) illustrates the case with different  $L_x$  but fixed  $L_y$  while Fig. 4(c) shows the case with different  $L_y$  but fixed  $L_x$ . Both  $d_{33}^*$  and  $\kappa_{33}^*$  of the  $a_1^+c^+/a_2^+c^+$  superdomains show a consistent, nonlinear  $L_x$ -dependence in Fig.4(b). Enhancement of up to 11% for  $d_{33}^*$  and 27% for  $\kappa_{33}^*$  is estimated when  $L_x$  increases from 19.2 nm to 31.2 nm at a fixed  $L_y$  =128 nm. When  $L_y$  varies while keeping  $L_x$  fixed, both  $d_{33}^*$  and  $\kappa_{33}^*$  show opposite domain size dependences as seen in Fig.4(d). Specifically, both  $d_{33}^*$  and  $\kappa_{33}^*$  drop nonlinearly by 22% and 51%, respectively, with  $L_y$  changing from 96 nm to 192 nm with  $L_x$  kept as 25.6 nm.

By comparing Fig. 2 and Fig. 4, we find that  $d_{33}^*$  and  $\kappa_{33}^*$  always show a consistent domain size dependence in both types of superdomain structures. Moreover, for both types of superdomain structures,  $d_{33}^*$  and  $\kappa_{33}^*$  increases when the polydomain size (i.e.,  $L_x$ ) increases but decreases when the superdomain size (i.e.,  $L_y$ ) increases.

#### 4. Discussion

#### 4.1 Local piezoresponses from domain variants and domain walls

To understand the domain size effects on the overall responses, we separately evaluated the local dielectric and piezoelectric contributions from each type of domain variants, domain walls, and superdomain walls. We find that the local polarization responses ( $\Delta P_3$ ) and strain responses ( $\Delta \varepsilon_{33}$ ) are highly inhomogeneous and show strong spatial variations along the outof-plane direction of the film. Taking the  $a_1^+a_2^+/a_2^+c^+//a_1^-a_2^+/a_2^+c^+$  superdomains with  $L_x =$ 32nm,  $L_y = 128$ nm as an example, we plotted the ferroelectric polarization under zero electric field (Fig. 5(a-c)), polarization responses  $\Delta P_3$  (Fig. 5(d-f)) and strain responses  $\Delta \varepsilon_{33}$  (Fig. 5(gi)) under the applied electric field of 0.1 MV/m in the x-y plane cross sections at the top (z =33), middle (z = 23), and bottom (z = 14) of the film. In Fig. 5(a-c), the black arrows represent the in-plane polarization direction and the color corresponds the value of the out-of-plane polarization  $P_3$ , from which the  $a_2c$  and  $a_1a_2$  domains can be distinguished, as labeled in Fig. 5(a). We observe that the polarization distribution inside each domain is more uniform at the top layer than that at the bottom layer. From the film top to bottom,  $P_3$  inside the  $a_2c$  domains reduces while  $P_3$  inside the  $a_1a_2$  domains increases. As a result, the polarization directions of the  $a_1^+a_2^+$  and  $a_1^-a_2^+$  domains are no longer strictly in-plane, i.e., pointing toward [110] and [ $\bar{1}10$ ] directions, but show a triclinic distortion, i.e.,  $P_1 \neq 0$ ,  $P_2 \neq 0$ ,  $P_3 \neq 0$ . The distortion

becomes stronger approaching the film bottom. Moreover, the superdomain wall in the middle layer shows a zig-zag morphology, which is different from those at the top and bottom layers. This disruption at the superdomain walls have been discussed in our previous work[38].

As a result of the layer-dependent polarization distributions,  $\Delta P_3$  and  $\Delta \varepsilon_{33}$  inside each domain variants also become highly inhomogeneous, as shown in Fig.5 (d-f) and Fig.5 (g-i), respectively. The  $\Delta P_3$  inside the  $a_1^+ a_2^+$  and  $a_1^- a_2^+$  domain variants are higher than that of the  $a_2^+c^+$  domain variant at all layers, especially at the middle layer. Peak values of  $\Delta P_3$  can be found at the domain walls between an  $a_1a_2$ -type domain and an  $a_2^+c^+$  domain, especially near the superdomain wall. Interestingly, for each  $a_1a_2$ -type domain, the polarization responses are different at the adjacent domain walls, and these differences also depends on the layers. For example, the right-hand-side domain wall of the  $a_1^-a_2^+$  domain (circled in red in Fig. 5(f)) is associated with a peak  $\Delta P_3$  while the left-hand-side domain wall has no enhancement in  $\Delta P_3$ . These inequivalent behaviors of the adjacent domain walls are likely due to the fact the  $a_1a_2/a_1c$  domain walls are inclined with respect to the in-plane direction. Similar asymmetry of local responses at a pair of domain walls have been reported in other inclined domain walls in ferroelectric thin films, such as the 90-degree a/c domain walls in PbTiO<sub>3</sub> [48] and 71-degree domain walls in BiFeO<sub>3</sub> [49].

The out-of-plane strain responses,  $\Delta \varepsilon_{33}$ , also display strong spatial inhomogeneity and layer dependence, as shown in Fig.5 (g-i). In the top layer (Fig. 5g), the  $a_2^+c^+$  domains have positive  $\Delta \varepsilon_{33}$  while the  $a_1a_2$ -type domains show negative ones. The  $\Delta \varepsilon_{33}$  at domain walls is higher than those inside domain, and the peak values of  $\Delta \varepsilon_{33}$  occur near the superdomain wall. In the middle layer (Fig. 5h), the  $\Delta \varepsilon_{33}$  inside the domains become more uniform while the

domain wall contributions exhibit asymmetry with respect to the left- and right-hand-side of a domain. This asymmetry becomes more significant in the bottom layer (Fig. 5i) wherein one of the pair of domain walls has negligible  $\Delta \varepsilon_{33}$  whereas the other one has a strong positive  $\Delta \varepsilon_{33}$ . The spatial dependence of  $\Delta \varepsilon_{33}$  is to some extent correlated with that of  $\Delta P_3$  but with slight deviations locally.

Fig. 5 indicates that the local polarization and strain responses to the applied field are highly layer dependent, making it less accurate to represent the domain and domain wall contributions merely by using the averaged local responses across the entire film thickness. Therefore, we performed a layer-resolved analysis for all simulation results in Fig. 2d (i.e., fixed  $L_x = 32$  nm and different  $L_y$ ) by averaging the total responses from each type of domains and domain walls within each layer, and plotted them against the layer number in Fig. 6. For the total response in each layer (Fig.6(a)), there is a quasi-linear decrease of  $\Delta P_3$  from the film bottom to the top, along with drops at the two ends. Higher  $\Delta P_3$  is seen when  $L_y$  decreases, which agrees with the domain size dependence of  $\kappa_{33}^*$  and  $d_{33}^*$  shown in Fig. 2. The contribution from  $a_1^+a_2^+$  domains (Fig.6 (b)) have consistent trends as the total responses in terms of the  $L_y$  and layer dependences. The other in-plane domain variant  $a_1^-a_2^+$  show similar behavior and thus is omitted here. In contrast, the out-of-plane domain variants  $a_2^+c$  (Fig.6(c)) shows an irregular layer dependence and relatively small magnitudes than that of the  $a_1a_2$ -type domain variants. The contributions from the domain walls, though exhibiting the largest magnitude, show opposite layer dependence to that of the total response and less definite size dependence. Comparing Fig. 6(b-d) with Fig. 6(a), we conclude that the domain size effects on  $\kappa_{33}^*$  and  $d_{33}^*$  for the  $a_1^+ a_2^+ / a_2^+ c^+ / / a_1^- a_2^+ / a_2^+ c^+$  superdomain structures may be dominated by the local responses from the  $a_1a_2$ -type domains.

We further performed similar layer-resolved analyses to other measures of dielectric and piezoelectric responses induced by the applied field  $E_3 = 0.1$  MV/m, including the variation of the out-of-plane strain  $\Delta \varepsilon_{33}$ , the out-of-plane polarization  $\Delta P_3$ , the polarization modulus  $\Delta | \mathbf{P} |$ and the rotation angle  $\theta$  under an external electric field of. The choice of the latter two factors are inspired by the well-established model of polarization rotation and polarization elongation as the two major contributors to intrinsic piezoelectric responses in perovskite piezoelectric crystals [7]. To find the quantity most relevant to the overall piezoelectric response, we computed the layer-resolved correlation coefficient R between the  $L_y$ -dependence of  $d_{33}^*$  and the  $L_{V}$ -dependence of the four factors ( $\Delta \varepsilon_{33}$ ,  $\Delta P_{3}$ ,  $\Delta |\mathbf{P}|$  and  $\theta$ ). For each factor, it is averaged over the entire layer, the region of three domain variants  $(a_1^+a_2^+, a_1^-a_2^+)$  and  $a_2^+c$  domain), and the domain wall region. Therefore, we define twenty factors in total and computed the correlations between their domain size  $(L_y)$  dependence and the  $L_y$ -dependence of  $d_{33}^*$ . We also computed the correlation coefficients for the twenty factors averaged over the entire film, as shown in the bottom of Fig. 7. The correlation coefficient R between the  $L_y$ -dependence of factor X (X can be  $\Delta \varepsilon_{33}$ ,  $\Delta P_3$ ,  $\Delta |P|$  and  $\theta$  of any type of the three domain variants or domain walls) at a given layer Z, denoted as  $X(L_y, Z)$ , and the  $L_y$ -dependence of  $d_{33}^*$ , denoted as  $d_{33}^*$  $(L_y)$ , is calculated as

$$R = \frac{\operatorname{cov}(d_{33}^*(L_y), X(L_y, Z))}{\sigma(d_{33}^*(L_y))\sigma(X(L_y, Z))},$$

where  $cov(d_{33}^*(L_y), X(L_y, Z))$  is the covariance between  $d_{33}^*(L_y)$  and  $X(L_y, Z)$ , and  $\sigma(d_{33}^*(L_y))$  and  $\sigma(X(L_y, Z))$  represent the standard deviation of  $d_{33}^*(L_y)$  and  $d_{33}^*($ 

Fig. 7 shows dominant positive correlation between the  $L_y$ -dependence of  $\Delta P_3$  with that of  $d_{33}$ , which can be attributed to the strong correlation between  $\Delta P_3$  and  $d_{33}$  of the two in-plane domain variants at all layers, i.e.  $\Delta P_3^{a_1^+a_2^+}$  and  $\Delta P_3^{a_1^-a_2^+}$ . In contrast, the correlations for the out-of-domain variant  $\Delta P_3^{a_2^+c^+}$  and domain wall  $\Delta P_3^{DW}$  are weaker due to variations among different layers as also observed in Fig.6(c-d). The  $\Delta \varepsilon_{33}^{layer}$  of the overall film show consistent domain size dependence as the  $d_{33}^+$  despite of fluctuations among layers. The  $\Delta \varepsilon_{33}^{DW}$  of the overall film is the only one factor that exhibits strongly negative correlation, suggesting that the strain response at the DWs may not be a critical factor to determine the domain size dependence of the piezoelectricity. All the  $\Delta |P|$ 's show positive correlations despite of moderate layer dependences, while all the  $\Delta \theta$ 's generally show weaker positive correlation than do the  $\Delta |P|$ 's. By reorganizing the columns of the R matrix in terms of the types of domain variants and domain walls (Fig.S2), we can identify that the  $a_1a_2$ -type domains generally show consistent domain size dependence as that of the overall  $d_{33}^*$ , suggesting the dominant contributions to the overall responses from the  $a_1a_2$ -type domain variants.

In summary, despite of the complexity associated with the layer fluctuation of several factors, our statistical analysis reveals that the change in the out-of-plane polarization serves as

the primary microscopic mechanism to account for the domain size dependent of piezoelectricity for the  $a_1a_2/a_2c$ -type superdomain structures, and the  $a_1a_2$ -type domains make the primary contributions.

#### 4.2 Contribution of polydomains and superdomains to the domain size effects

We discuss the contribution of superdomains to the overall  $d_{33}^*$  as compared to a single bundle of polydomains. To this end, we consider two types of domain structures, namely, the  $a_1c/a_2c$ -type superdomains constituted by two alternating bundles of  $a_1^-c^+/a_2^+c^+$  and  $a_1^+c^+/a_2^+c^+$  polydomains (Fig. 8(a)) and the single-bundle  $a_1^+c^+/a_2^+c^+$  polydomains (Fig. 8(b)). A series of domain structures with fixed  $L_y = 156$  nm and varied  $L_x$  have been constructed and relaxed to the equilibrium under misfit strain  $\varepsilon_{11}^{mis} = \varepsilon_{22}^{mis} = 0.075\%$  at 400K. The domain size ( $L_x$ ) dependence of  $d_{33}^*$  are evaluated and plotted in Fig. 8(b) for  $L_x$  ranges from 18 to 32 nm. Instead of showing the absolute value of  $d_{33}^*$ , we present the relative difference,  $\Delta d_{33}^*$ , with respect to the minima of each case. We find that  $\Delta d_{33}^*$  of the single-bundle polydomain structure is generally smaller than that of the superdomain structure and fluctuates around 1.0 pC/N. In contrast,  $\Delta d_{33}^*$  of the superdomain structure continuously increases up to 11 pC/N. This result indicates that the presence of superdomains can remarkably increase the domain size effect, which is likely to due to the formation of superdomain walls associated with highly inhomogeneous polarization [38].

## 4.3 Tuning the domain size dependence of $d_{33}^*$ by misfit strains and temperature

One question of immediate experimental interest is that whether the domain size effect in the thin films can be tuned. Here, we demonstrate the possibility to modulate the domain size effect by engineering the misfit strains and the polymorphic phase boundaries of KNN. Take the  $a_1^+c^+/a_2^+c^+$  superdomain as an example, we evaluate the domain size effects of the same

structure at different misfit strains and temperatures, as shown in Fig. 9. The choice of the misfit strains and temperatures are guided by the temperature-misfit strain phase diagrams for (001)-oriented KNN thin films subject to equal-biaxial misfit strains (Fig. 9(a), replotted from Ref. [43]). In all cases with varied misfit strains shown in Fig. 9(a), we have examined that the preset domain sizes are maintained and not changed by the misfit strains. And the relative changes of  $d_{33}^*$  in each case,  $\Delta d_{33}^*$ , are plotted for better comparison. We find that, with  $\varepsilon_{11}^{mis}$  changing from -0.5% to 0.075% to approach the mix-phase region in the phase diagram,  $\Delta d_{33}^*$  increases from a negligible value to more than 20 pC/N (Fig. 9(b)). Moreover, when both the misfit strain and the temperature are changed to approach the phase boundary of the  $R_D$  phase region,  $\Delta d_{33}^*$  can also be enhanced remarkably (Fig. 9(c)). These two examples demonstrate that stronger domain size effect of piezoelectricity can be expected near a ferroelectric-ferroelectric phase transformation, which is consistent with the findings in ferroelectric bulk crystals [27]. Moreover, this finding suggests the possibility to achieve stronger domain size effect by engineering a ferroelectric polymorphic phase boundary to room temperature, e.g., by doping[50] or strain engineering[45].

We should point out that, in-principle, the equilibrium domain size in a ferroelectric thin film is correlated to the film thickness due to the competition between electrostatic, elastic energy and domain wall energies, following the Kittel's law[51–53]. In this work, we kept the film thickness as a constant when varying the domain size to isolate the effect of domain size change to the dielectric and piezoelectric responses and eliminate that from the change of film thickness. In reality, for a film with a given thickness, the same type of domain structure with different domain periods may correspond a series of metastable states associated with excessive electrostatic and/or elastic energies. In principles, these metastable states can be obtained by a careful control of local domains, e.g., via scanning probe techniques [54]. The covariation of film thicknesses and domain sizes and its effect on the domain size dependence of piezoelectric responses require more careful and in-depth consideration and will be examined in a future

publication. Notably, recent experiments have demonstrated continuous control of the domain size in one of the superdomain structures of  $K_xNa_{1-x}NbO_3$  thin films [51], which provides possibility to validate our theoretical predictions.

#### 4.4 The influence of flexoelectric effect on the piezoelectric response

As shown in Fig. 5, the polarization and strain distributions are highly inhomogeneous in the  $a_1c/a_1a_2$ -type superdomain structure. It is expected that the flexoelectric effect, i.e., coupling between polarization and strain gradients, may be significant and contribute to the piezoelectric responses. To quantify the flexoelectric contribution, we performed additional phase-field simulations with considering the flexoelectric effect following Ref. [55]. The detailed description of the method and choice of the flexoelectric coefficients are given in Supporting Information Note 1.

Fig. S3(a-c) show the difference of the local out-of-plane strain responses in the middle layer of the KNN thin film under an applied field  $E_3 = 0.1 \,\mathrm{MV/m}$  with and without considering the flexoelectric effect ( $\Delta \varepsilon_{33}^{\mathrm{flexo}} - \Delta \varepsilon_{33}^{\mathrm{no-flexo}}$ ). It is found that all three independent components of the flexoelectric tensor, i.e., the longitudinal  $f_{11}$ , transverse  $f_{12}$ , and shear  $f_{44}$  components, can influence the local strain response and in different ways. Specifically,  $f_{11}$  mainly impacts the domain walls of the twin polydomains, i.e., between  $a_1^+ a_2^+$  and  $a_2^+ c^+$  or  $a_1^- a_2^+$  and  $a_2^+ c^+$ . In contrast,  $f_{12}$  mainly influences the superdomain walls between polydomains. For  $f_{44}$ , the variation is pronounced at both domain wall and superdomain wall regions. Notably,  $f_{12}$  and  $f_{44}$  generally have larger impacts on the local piezoelectric response than that from  $f_{11}$ , as indicated by the order of magnitude of  $\Delta \varepsilon_{33}^{\mathrm{flexo}} - \Delta \varepsilon_{33}^{\mathrm{no-flexo}}$ .

We also compared the overall out-of-plane effective piezoelectric coefficient,  $d_{33}^*$ , for the three cases with flexoelectricity and the case without flexoelectricity. We found that the variation of  $d_{33}^*$  is negligible (< 2 pC/N, ~ 1%), as shown in Fig.R1(d). This may be explained by the fact that the local strain responses induced by flexoelectricity have positive and negative variations of comparable magnitude, which cancel out macroscopically. Therefore, the flexoelectric effect was neglected in all other simulations in this work.

In fact, the impact of flexoelectricity on the polarization and domain structures in

ferroelectrics at nanoscale will be more complex, such as widening of domain wall thickness, distortion of domain walls near surface, and vortex-like structures [56,57], which may also appear in the superdomain structures of KNN thin films and lead to unique piezoelectric responses. These interesting topics remain open questions to be explored systematically in future research.

#### 5. Conclusion

In this work, we performed phase-field simulations to evaluate the domain size dependence of piezoelectric and dielectric response ( $d_{33}^*$  and  $\kappa_{33}^*$ ) in KNN thin films with two representative superdomain structures. It shows that  $d_{33}^*$  and  $\kappa_{33}^*$  can either increase or decrease with reduced domain size, suggesting that the domain size effect is not universal in ferroelectric thin film, similar to that for the bulk piezoelectric crystals. The simulation results reveal highly inhomogeneous and layer-dependent behavior for the local piezoelectric and dielectric responses inside the domains. Layer-resolved statistical analyses on four key factors of the local responses ( $\Delta \varepsilon_{33}$ ,  $\Delta P_3$ ,  $\Delta |P|$  and  $\theta$ ) suggest that the domain size effect in the  $a_1a_2/a_2c$ -type superdomains is dominated by the out-of-plane polarization variation  $\Delta P_3$  of the  $a_1a_2$ -type domain variants. We also find that the domain size dependence is more pronounced near a polymorphic phase boundary, suggesting tunability of the domain size effect by chemical doping and misfit strain engineering. The domain size effect is shown to be enhanced with the presence of superdomain walls, indicating a new routine to enhance materials properties by the largely unexplored superdomain engineering.

#### 6. Acknowledgement

This work was supported by the NSF of China (Grant No. 52102141) and the NSF of Hubei Province (2021CFB051). The work is also supported by the Fundamental Research Funds for the Central Universities. M.J.Z. also acknowledge the fundings by Wuhan Talents program. B.W. acknowledges support by the National Science Foundation through Grant No. DMR-1744213. Part of this work was performed under the auspices of the U.S. Department of Energy by Lawrence Livermore National Laboratory under Contract DE-AC52-07NA27344 (B.W.).

#### References

- [1] S. Zhang, F. Li, F. Yu, X. Jiang, H.Y. Lee, J. Luo, T.R. Shrout, Recent developments in piezoelectric crystals, J. Korean Ceram. Soc. 55 (2018) 419–439. https://doi.org/10.4191/kcers.2018.55.5.12.
- [2] S. Trolier-McKinstry, S. Zhang, A.J. Bell, X. Tan, High-Performance Piezoelectric Crystals, Ceramics, and Films, Annu. Rev. Mater. Res. 48 (2018) 191–217. https://doi.org/10.1146/annurev-matsci-070616-124023.
- [3] C. Qiu, B. Wang, N. Zhang, S. Zhang, J. Liu, D. Walker, Y. Wang, H. Tian, T.R. Shrout, Z. Xu, L.Q. Chen, F. Li, Transparent ferroelectric crystals with ultrahigh piezoelectricity, Nature. 577 (2020) 350–354. https://doi.org/10.1038/s41586-019-1891-y.
- [4] H. Leng, Y. Yan, B. Wang, T. Yang, H. Liu, X. Li, R. Sriramdas, K. Wang, M. Fanton, R.J. Meyer, L.-Q. Chen, S. Priya, High performance high-power textured Mn/Cu-doped PIN-PMN-PT ceramics, Acta Mater. 234 (2022) 118015. https://doi.org/10.1016/j.actamat.2022.118015.
- [5] J. Rödel, W. Jo, K.T.P. Seifert, E.M. Anton, T. Granzow, D. Damjanovic, Perspective on the development of lead-free piezoceramics, J. Am. Ceram. Soc. 92 (2009) 1153– 1177. https://doi.org/10.1111/j.1551-2916.2009.03061.x.
- [6] D. Damjanovic, Ferroelectric, dielectric and piezoelectric properties of ferroelectric thin films and ceramics, Reports Prog. Phys. 61 (1998) 1267–1324. https://doi.org/10.1088/0034-4885/61/9/002.
- [7] D. Damjanovic, Contributions to the piezoelectric effect in ferroelectric single crystals and ceramics, J. Am. Ceram. Soc. 88 (2005) 2663–2676. https://doi.org/10.1111/j.1551-2916.2005.00671.x.
- [8] M. Davis, M. Budimir, D. Damjanovic, N. Setter, Rotator and extender ferroelectrics: Importance of the shear coefficient to the piezoelectric properties of domainengineered crystals and ceramics, J. Appl. Phys. 101 (2007) 054112. https://doi.org/10.1063/1.2653925.
- [9] B. Wang, Y. Gu, S. Zhang, L.-Q. Chen, Flexoelectricity in solids: Progress,

- challenges, and perspectives, Prog. Mater. Sci. 106 (2019) 100570. https://doi.org/10.1016/j.pmatsci.2019.05.003.
- [10] C. Hu, X. Meng, M.-H. Zhang, H. Tian, J.E. Daniels, P. Tan, F. Huang, L. Li, K. Wang, J.-F. Li, Q. Lu, W. Cao, Z. Zhou, Ultra-large electric field-induced strain in potassium sodium niobate crystals., Sci. Adv. 6 (2020) eaay5979. https://doi.org/10.1126/sciadv.aay5979.
- [11] M. Davis, D. Damjanovic, N. Setter, Electric-field-, temperature-, and stress-induced phase transitions in relaxor ferroelectric single crystals, Phys. Rev. B. 73 (2006) 014115. https://doi.org/10.1103/PhysRevB.73.014115.
- [12] H. Liu, H. Wu, K.P. Ong, T. Yang, P. Yang, P.K. Das, X. Chi, Y. Zhang, C. Diao, W.K.A. Wong, E.P. Chew, Y.F. Chen, C.K.I. Tan, A. Rusydi, M.B.H. Breese, D.J. Singh, L.-Q. Chen, S.J. Pennycook, K. Yao, Giant piezoelectricity in oxide thin films with nanopillar structure., Science. 369 (2020) 292–297. https://doi.org/10.1126/science.abb3209.
- [13] M. Höfling, X. Zhou, L.M. Riemer, E. Bruder, B. Liu, L. Zhou, P.B. Groszewicz, F. Zhuo, B.-X. Xu, K. Durst, X. Tan, D. Damjanovic, J. Koruza, J. Rödel, Control of polarization in bulk ferroelectrics by mechanical dislocation imprint., Science. 372 (2021) 961–964. https://doi.org/10.1126/science.abe3810.
- [14] F. Zhuo, X. Zhou, S. Gao, M. Höfling, F. Dietrich, P.B. Groszewicz, L. Fulanović, P. Breckner, A. Wohninsland, B. Xu, H. Kleebe, X. Tan, J. Koruza, D. Damjanovic, J. Rödel, Anisotropic dislocation-domain wall interactions in ferroelectrics, Nat. Commun. 13 (2022) 6676. https://doi.org/10.1038/s41467-022-34304-7.
- [15] D.-S. Park, M. Hadad, L.M. Riemer, R. Ignatans, D. Spirito, V. Esposito, V. Tileli, N. Gauquelin, D. Chezganov, D. Jannis, J. Verbeeck, S. Gorfman, N. Pryds, P. Muralt, D. Damjanovic, Induced giant piezoelectricity in centrosymmetric oxides., Science. 375 (2022) 653–657. https://doi.org/10.1126/science.abm7497.
- [16] G. Arlt, The influence of microstructure on the properties of ferroelectric ceramics, Ferroelectrics. 104 (1990) 217–227. https://doi.org/10.1080/00150199008223825.
- [17] G. Arlt, The role of domain walls on the dielectric, elastic and piezoelectric properties

- of ferroelectric ceramics, Ferroelectrics. 76 (1987) 451–458. https://doi.org/10.1080/00150198708016967.
- [18] V. Buscaglia, C.A. Randall, Size and scaling effects in barium titanate. An overview, J. Eur. Ceram. Soc. 40 (2020) 3744–3758. https://doi.org/10.1016/j.jeurceramsoc.2020.01.021.
- [19] S. Wada, K. Muraoka, H. Kakemoto, T. Tsurumi, H. Kumagai, Enhanced piezoelectric properties of potassium niobate single crystals by domain engineering, Japanese J. Appl. Physics, Part 1 Regul. Pap. Short Notes Rev. Pap. 43 (2004) 6692–6700. https://doi.org/10.1143/JJAP.43.6692.
- [20] S. Wada, K. Yako, H. Kakemoto, T. Tsurumi, T. Kiguchi, Enhanced piezoelectric properties of barium titanate single crystals with different engineered-domain sizes, J. Appl. Phys. 98 (2005) 014109. https://doi.org/10.1063/1.1957130.
- [21] D. Lin, H.J. Lee, S. Zhang, F. Li, Z. Li, Z. Xu, T.R. Shrout, Influence of domain size on the scaling effects in Pb(Mg1/3Nb2/3)O3–PbTiO3 ferroelectric crystals, Scr. Mater. 64 (2011) 1149–1151. https://doi.org/10.1016/j.scriptamat.2011.03.018.
- [22] D. Lin, S. Zhang, C. Cai, W. Liu, Domain size engineering in 0.5%MnO2-(K0.5Na0.5)NbO3 lead free piezoelectric crystals, J. Appl. Phys. 117 (2015) 074103. https://doi.org/10.1063/1.4913208.
- [23] D. Lin, S. Zhang, Z. Li, F. Li, Z. Xu, S. Wada, J. Luo, T.R. Shrout, Domain size engineering in tetragonal Pb(In1/2Nb1/2)O3 -Pb(Mg1/3Nb2/3)O3-PbTiO3 crystals, J. Appl. Phys. 110 (2011) 084110. https://doi.org/10.1063/1.3654137.
- [24] Y. Xiang, R. Zhang, W. Cao, Optimization of piezoelectric properties for [001]c poled 0.94Pb(Zn1/3Nb2/3)O3-0.06PbTiO3 single crystals, Appl. Phys. Lett. 96 (2010) 94–96. https://doi.org/10.1063/1.3314285.
- [25] T. Sluka, A.K. Tagantsev, D. Damjanovic, M. Gureev, N. Setter, Enhanced electromechanical response of ferroelectrics due to charged domain walls, Nat. Commun. 3 (2012) 748. https://doi.org/10.1038/ncomms1751.
- [26] J. Hlinka, P. Ondrejkovic, P. Marton, The piezoelectric response of nanotwinned BaTiO3., Nanotechnology. 20 (2009) 105709. https://doi.org/10.1088/0957-

- 4484/20/10/105709.
- [27] B. Wang, F. Li, L. Chen, Inverse Domain-Size Dependence of Piezoelectricity in Ferroelectric Crystals, Adv. Mater. 33 (2021) 2105071. https://doi.org/10.1002/adma.202105071.
- [28] N. Bassiri-Gharb, I. Fujii, E. Hong, S. Trolier-McKinstry, D. V. Taylor, D. Damjanovic, Domain wall contributions to the properties of piezoelectric thin films, J. Electroceramics. 19 (2007) 49–67. https://doi.org/10.1007/s10832-007-9001-1.
- [29] J.F. Ihlefeld, D.T. Harris, R. Keech, J.L. Jones, J.P. Maria, S. Trolier-McKinstry, Scaling Effects in Perovskite Ferroelectrics: Fundamental Limits and Process-Structure-Property Relations, J. Am. Ceram. Soc. 99 (2016) 2537–2557. https://doi.org/10.1111/jace.14387.
- [30] V.G. Koukhar, N.A. Pertsev, R. Waser, Thermodynamic theory of epitaxial ferroelectric thin films with dense domain structures, Phys. Rev. B. 64 (2001) 214103. https://doi.org/10.1103/PhysRevB.64.214103.
- [31] M.-J. Zhou, J.-J. Wang, L.-Q. Chen, C.-W. Nan, Strain, temperature, and electric-field effects on the phase transition and piezoelectric responses of K0.5Na0.5NbO3 thin films, J. Appl. Phys. 123 (2018) 154106. https://doi.org/10.1063/1.5027505.
- [32] F. Griggio, S. Jesse, A. Kumar, O. Ovchinnikov, H. Kim, T.N. Jackson, D. Damjanovic, S. V. Kalinin, S. Trolier-McKinstry, Substrate Clamping Effects on Irreversible Domain Wall Dynamics in Lead Zirconate Titanate Thin Films, Phys. Rev. Lett. 108 (2012) 157604. https://doi.org/10.1103/PhysRevLett.108.157604.
- [33] A. Brewer, S. Lindemann, B. Wang, W. Maeng, J. Frederick, F. Li, Y. Choi, P.J. Thompson, J.W. Kim, T. Mooney, V. Vaithyanathan, D.G. Schlom, M.S. Rzchowski, L.Q. Chen, P.J. Ryan, C.B. Eom, Microscopic piezoelectric behavior of clamped and membrane (001) PMN-30PT thin films, Appl. Phys. Lett. 119 (2021) 202903. https://doi.org/10.1063/5.0068581.
- [34] S. Trolier-Mckinstry, P. Muralt, Thin film piezoelectrics for MEMS, J. Electroceramics. 12 (2004) 7–17. https://doi.org/10.1023/B:JECR.0000033998.72845.51.

- [35] J. Luo, W. Sun, Z. Zhou, Y. Bai, Z.J. Wang, G. Tian, D. Chen, X. Gao, F. Zhu, J.F. Li, Domain Evolution and Piezoelectric Response across Thermotropic Phase Boundary in (K,Na)NbO3-Based Epitaxial Thin Films, ACS Appl. Mater. Interfaces. 9 (2017) 13315–13322. https://doi.org/10.1021/acsami.7b02263.
- [36] J. Luo, W. Sun, Z. Zhou, H.-Y. Lee, K. Wang, F. Zhu, Y. Bai, Z.J. Wang, J.-F. Li, Monoclinic (K,Na)NbO3 Ferroelectric Phase in Epitaxial Films, Adv. Electron. Mater. 3 (2017) 1700226. https://doi.org/10.1002/aelm.201700226.
- [37] L. Hao, Y. Yang, Y. Huan, H. Cheng, Y.-Y. Zhao, Y. Wang, J. Yan, W. Ren, J. Ouyang, Achieving a high dielectric tunability in strain-engineered tetragonal K0.5Na0.5NbO3 films, Npj Comput. Mater. 7 (2021) 62. https://doi.org/10.1038/s41524-021-00528-2.
- [38] M.-J. Zhou, B. Wang, A. Ladera, L. Bogula, H.-X. Liu, L.-Q. Chen, C.-W. Nan, Phase diagrams, superdomains, and superdomain walls in KxNa1-xNbO3 epitaxial thin films, Acta Mater. 215 (2021) 117038. https://doi.org/10.1016/j.actamat.2021.117038.
- [39] Y.L. Li, S.Y. Hu, Z.K. Liu, L.Q. Chen, Effect of substrate constraint on the stability and evolution of ferroelectric domain structures in thin films, Acta Mater. 50 (2002) 395–411. https://doi.org/10.1016/S1359-6454(01)00360-3.
- [40] L.Q. Chen, Phase-field method of phase transitions/domain structures in ferroelectric thin films: A review, J. Am. Ceram. Soc. 91 (2008) 1835–1844. https://doi.org/10.1111/j.1551-2916.2008.02413.x.
- [41] Y.L. Li, S.Y. Hu, Z.K. Liu, L.Q. Chen, Effect of electrical boundary conditions on ferroelectric domain structures in thin films, Appl. Phys. Lett. 81 (2002) 427–429. https://doi.org/10.1063/1.1492025.
- [42] H. Pohlmann, J.-J. Wang, B. Wang, L.-Q. Chen, A thermodynamic potential and the temperature-composition phase diagram for single-crystalline K1-xNaxNbO3 (0 ≤ x ≤ 0.5), Appl. Phys. Lett. 110 (2017) 102906. https://doi.org/10.1063/1.4978360.
- [43] B. Wang, H.-N. Chen, J.-J. Wang, L.-Q. Chen, Ferroelectric domain structures and temperature-misfit strain phase diagrams of K1-xNaxNbO3 thin films: A phase-field study, Appl. Phys. Lett. 115 (2019) 092902. https://doi.org/10.1063/1.5116910.

- [44] M. Schmidbauer, L. Bogula, B. Wang, M. Hanke, L. von Helden, A. Ladera, J.-J. Wang, L.-Q. Chen, J. Schwarzkopf, Temperature dependence of three-dimensional domain wall arrangement in ferroelectric K0.9Na0.1NbO3 epitaxial thin films, J. Appl. Phys. 128 (2020) 184101. https://doi.org/10.1063/5.0029167.
- [45] L. von Helden, L. Bogula, P.-E. Janolin, M. Hanke, T. Breuer, M. Schmidbauer, S. Ganschow, J. Schwarzkopf, Huge impact of compressive strain on phase transition temperatures in epitaxial ferroelectric KxNa1–xNbO3 thin films, Appl. Phys. Lett. 114 (2019) 232905. https://doi.org/10.1063/1.5094405.
- [46] M. Schmidbauer, D. Braun, T. Markurt, M. Hanke, J. Schwarzkopf, Strain engineering of monoclinic domains in KxNa1–xNbO3 epitaxial layers: a pathway to enhanced piezoelectric properties, Nanotechnology. 28 (2017) 24LT02. https://doi.org/10.1088/1361-6528/aa715a.
- [47] W. Li, C. Chen, G. Xie, Y. Su, Optimizing K0.5Na0.5NbO3 Single Crystal by Engineering Piezoelectric Anisotropy, Nanomaterials. 11 (2021) 1753. https://doi.org/10.3390/nano11071753.
- [48] M. Li, B. Wang, H.J. Liu, Y.L. Huang, J. Zhang, X. Ma, K. Liu, D. Yu, Y.H. Chu, L.Q. Chen, P. Gao, Direct observation of weakened interface clamping effect enabled ferroelastic domain switching, Acta Mater. 171 (2019) 184–189. https://doi.org/10.1016/j.actamat.2019.04.003.
- [49] Y. Zhang, H. Lu, X. Yan, X. Cheng, L. Xie, T. Aoki, L. Li, C. Heikes, S.P. Lau, D.G. Schlom, L. Chen, A. Gruverman, X. Pan, Intrinsic Conductance of Domain Walls in BiFeO3., Adv. Mater. 31 (2019) 1902099. https://doi.org/10.1002/adma.201902099.
- [50] S. Zhang, Z. Zhou, J. Luo, J. Li, Potassium-Sodium-Niobate-Based Thin Films: Lead Free for Micro-Piezoelectrics, Ann. Phys. 531 (2019) 1800525. https://doi.org/10.1002/andp.201800525.
- [51] Y. Wang, S. Bin Anooz, G. Niu, M. Schmidbauer, L. Wang, W. Ren, J. Schwarzkopf, Thickness effect on ferroelectric domain formation in compressively strained K0.65Na0.35NbO3 epitaxial films, Phys. Rev. Mater. 6 (2022) 084413. https://doi.org/10.1103/PhysRevMaterials.6.084413.

- [52] Y. Feng, Y. Tang, D. Ma, Y. Zhu, M. Zou, M. Han, J. Ma, X. Ma, Thickness-Dependent Evolution of Piezoresponses and Stripe 90° Domains in (101)-Oriented Ferroelectric PbTiO3 Thin Films, ACS Appl. Mater. Interfaces. 10 (2018) 24627–24637. https://doi.org/10.1021/acsami.8b07206.
- [53] A.S. Everhardt, S. Damerio, J.A. Zorn, S. Zhou, N. Domingo, G. Catalan, E.K.H. Salje, L.-Q. Chen, B. Noheda, Periodicity-Doubling Cascades: Direct Observation in Ferroelastic Materials., Phys. Rev. Lett. 123 (2019) 087603. https://doi.org/10.1103/PhysRevLett.123.087603.
- [54] A. Gruverman, M. Alexe, D. Meier, Piezoresponse force microscopy and nanoferroic phenomena., Nat. Commun. 10 (2019) 1661. https://doi.org/10.1038/s41467-019-09650-8.
- [55] Y. Gu, M. Li, A.N. Morozovska, Y. Wang, E.A. Eliseev, V. Gopalan, L.-Q. Chen, Flexoelectricity and ferroelectric domain wall structures: Phase-field modeling and DFT calculations, Phys. Rev. B. 89 (2014) 174111. https://doi.org/10.1103/PhysRevB.89.174111.
- [56] A.N. Morozovska, R. Hertel, S. Cherifi-Hertel, V.Y. Reshetnyak, E.A. Eliseev, D.R. Evans, Chiral polarization textures induced by the flexoelectric effect in ferroelectric nanocylinders, Phys. Rev. B. 104 (2021) 054118. https://doi.org/10.1103/PhysRevB.104.054118.
- [57] A.N. Morozovska, E.A. Eliseev, S. V. Kalinin, R. Hertel, Flexosensitive polarization vortices in thin ferroelectric films, Phys. Rev. B. 104 (2021) 085420. https://doi.org/10.1103/PhysRevB.104.085420.

## Figures and captions

Figure 1

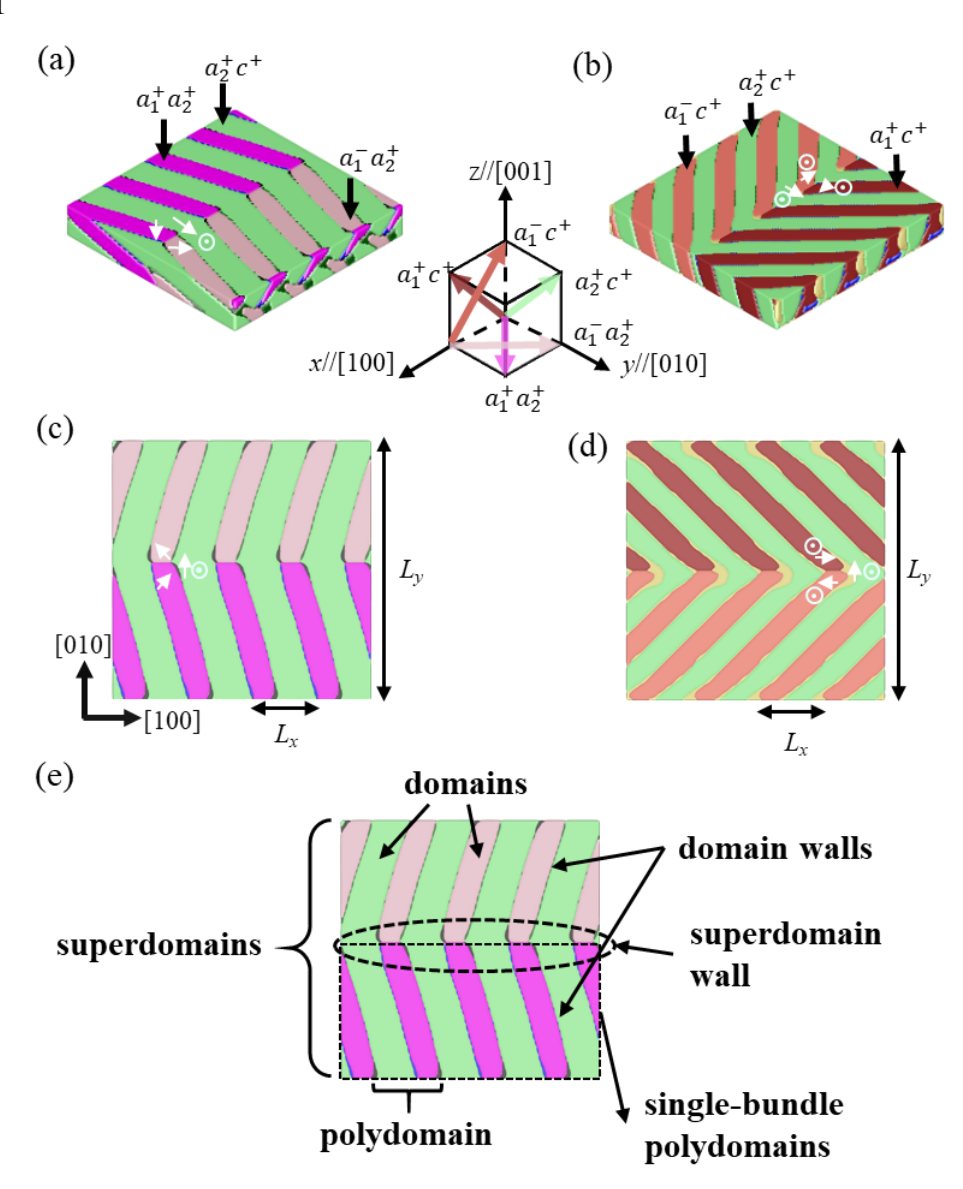


Fig.1 | Superdomain structures in (001)-oriented  $K_{0.5}Na_{0.5}NbO_3$  thin films by phase-field simulations. (a,c) the  $a_1a_2/a_2c$ -type superdomain structures and (b,d)  $a_1c/a_2c$ -type the superdomain structures visualized from (a,b) a 3-D orthographic view and (c,d) a planar view. The arrows in the graphs indicate the polarization directions in each domain variant. The inset in the center indicates the coordinate system of the 3-D graphs and the polarization directions of each domain variants with corresponding colors. The period of one pair of twin domains along [100] and [010] directions are labeled by  $L_x$  and  $L_y$ , respectively. (e) A schematic to distinguish some key concepts (superdomain, polydomain, single-bundle polydomains,

domains, superdomain walls and domain walls) for describing the domain structures in this work.

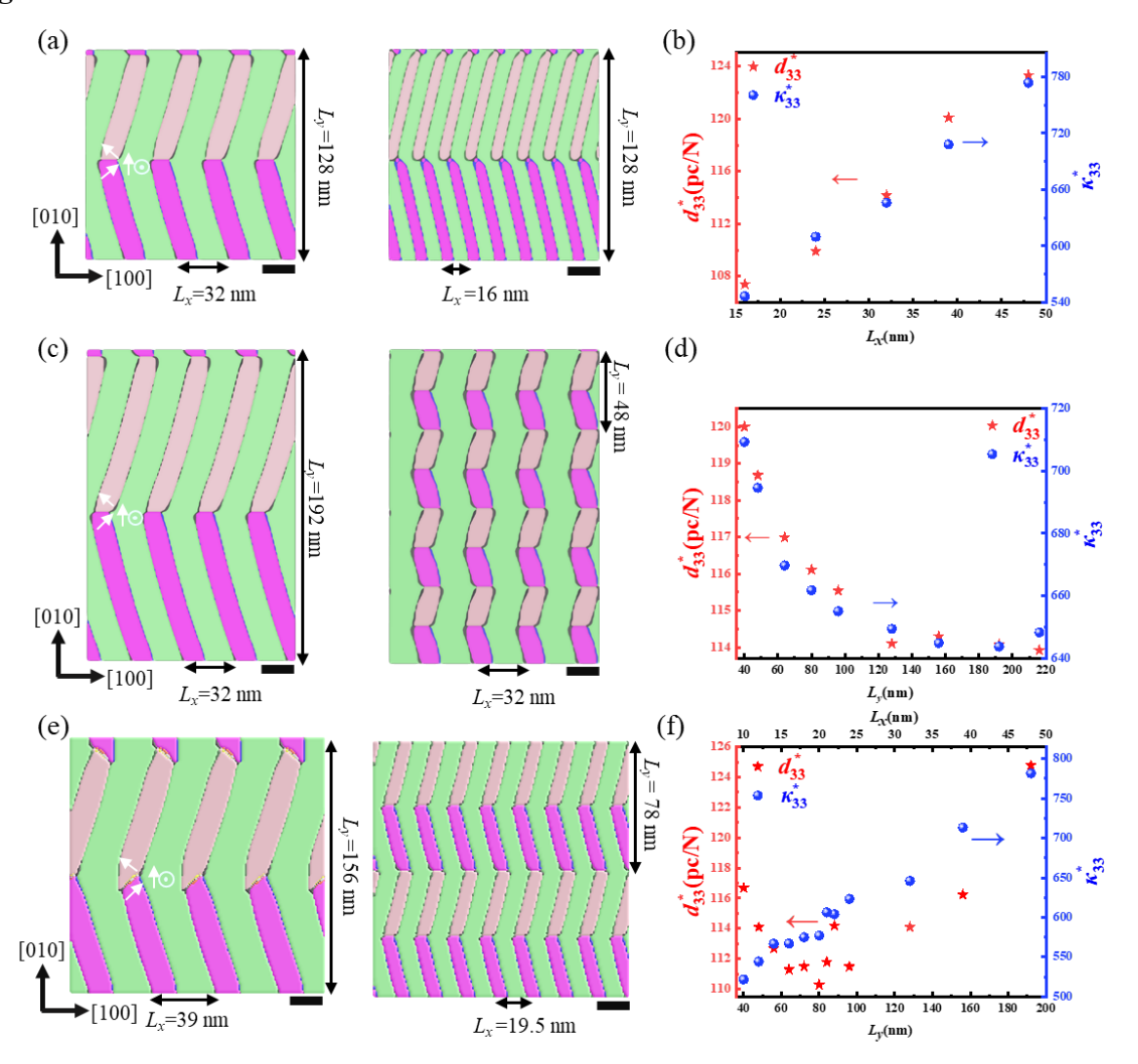


Fig.2 | Domain size effect on piezoelectric and dielectric properties of the  $a_1a_2/a_2c$ -type superdomains when the domain periods vary in one lateral direction. (a,c,e) Planar views of  $a_1a_2/a_2c$ -type superdomains with (a) different lateral period  $L_x$  but identical longitudinal period  $L_y$ , (c) different  $L_y$  but identical  $L_x$  and (e) varying  $L_x$  and  $L_y$  with a fix ratio of  $L_x$  /  $L_y$  = 1/4. The in-plane misfit strain is  $\varepsilon_{11}^{mis}$ = -0.4% and  $\varepsilon_{22}^{mis}$ = 1.0% and the temperature is 300 K. (b,d,f) The calculated out-of-plane piezoelectric coefficient  $d_{33}^*$  and dielectric constant  $\kappa_{33}^*$  as a function of (b)  $L_x$ ,(d)  $L_y$  and (f)  $L_y$  = 4  $L_x$ .

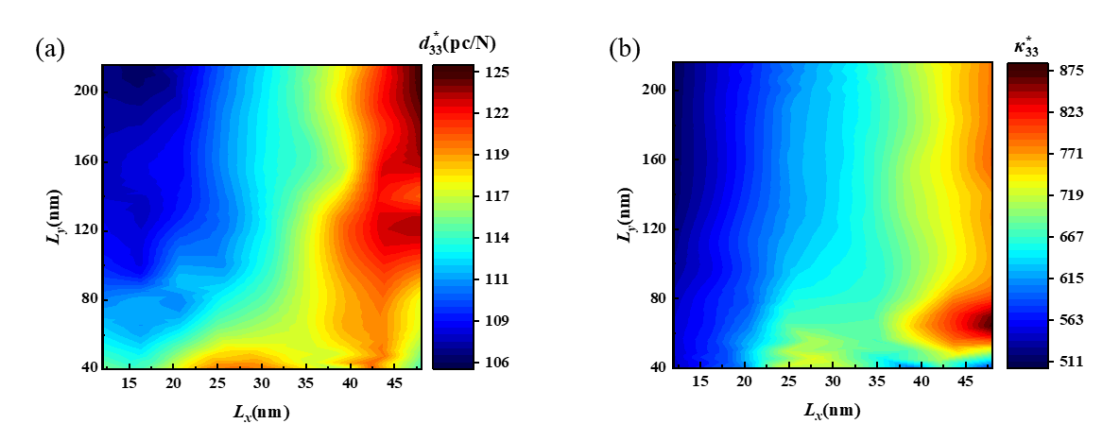


Fig.3 | The calculated mappings of piezoelectric and dielectric properties of the  $a_1a_2/a_2c$ -type superdomains at varying  $L_x$  and  $L_y$ . (a,b) The calculated out-of-plane (a) piezoelectric coefficient  $d_{33}^*$  and (b) dielectric constant  $\kappa_{33}^*$  as a function of  $L_x$  and  $L_y$ .

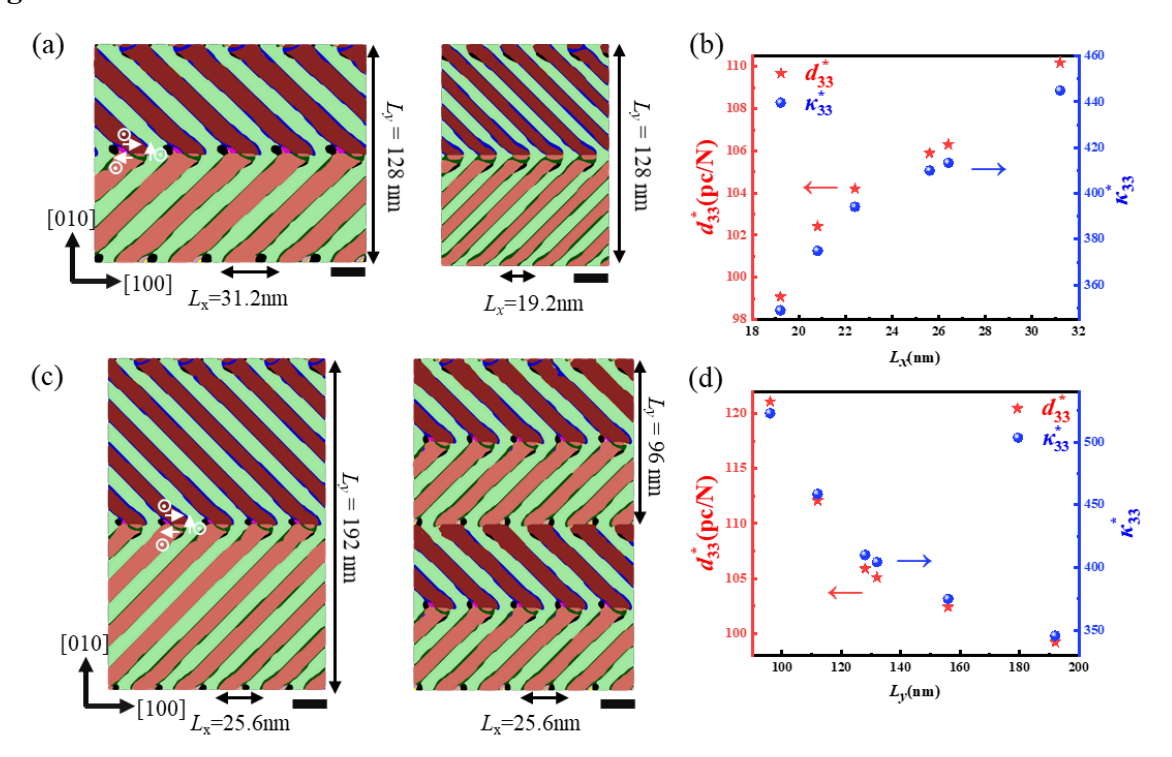


Fig.4 | Domain size effect on piezoelectric and dielectric properties of the  $a_1c/a_2c$ -type superdomains. (a,b) Planar views of stripe-like superdomains with (a) different lateral period  $L_x$  but identical longitudinal period  $L_y$  and (b) different  $L_y$  but identical  $L_x$ . The in-plane misfit strain is  $\varepsilon_{11}^{mis} = \varepsilon_{22}^{mis} = 0.075\%$  and the temperature is 400 K. (c,d) The calculated out-of-plane piezoelectric coefficient  $d_{33}^*$  and dielectric constant  $\kappa_{33}^*$  as a function of (c)  $L_x$  and (d)  $L_y$ .

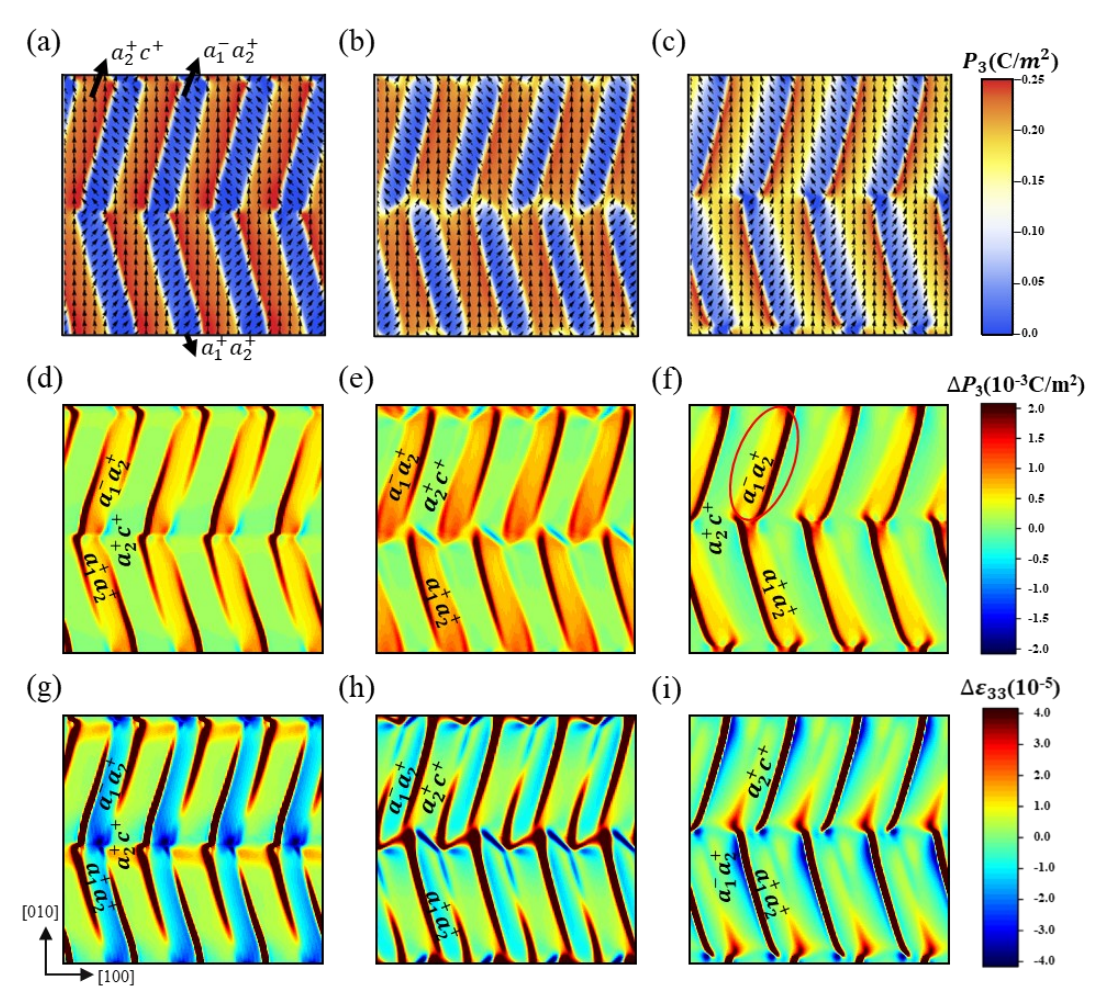


Fig.5 | The simulated (a - c) polarization distribution under zero electric field, (d - f) variation of out-of-plane polarization  $\Delta P_3$ , and (g - h) variation of out-of-plane strain  $\Delta \varepsilon_{33}$  at the (a,d,g) top, (b,e,h) middle and (c,f,i) bottom layers of the KNN thin film.

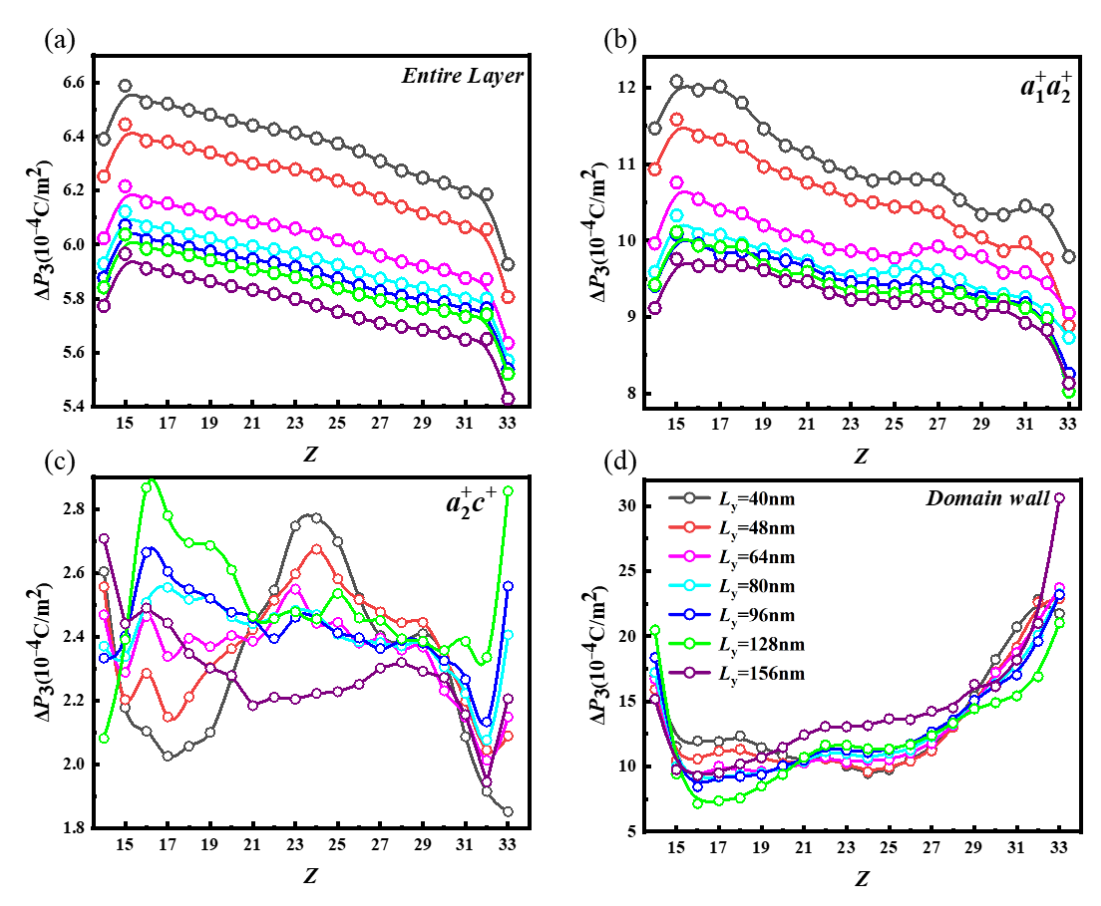


Fig.6 | The out-of-plane polarization  $\Delta P_3$  of the KNN thin film at different layers. The average variation of out-of-plane strain  $\Delta P_3$  of (a) entire layer and (b)  $a_1^+ a_2^+$  domain variants (c)  $a_2^+ c^+$  domain variants and (d) domain wall.

Figure 7

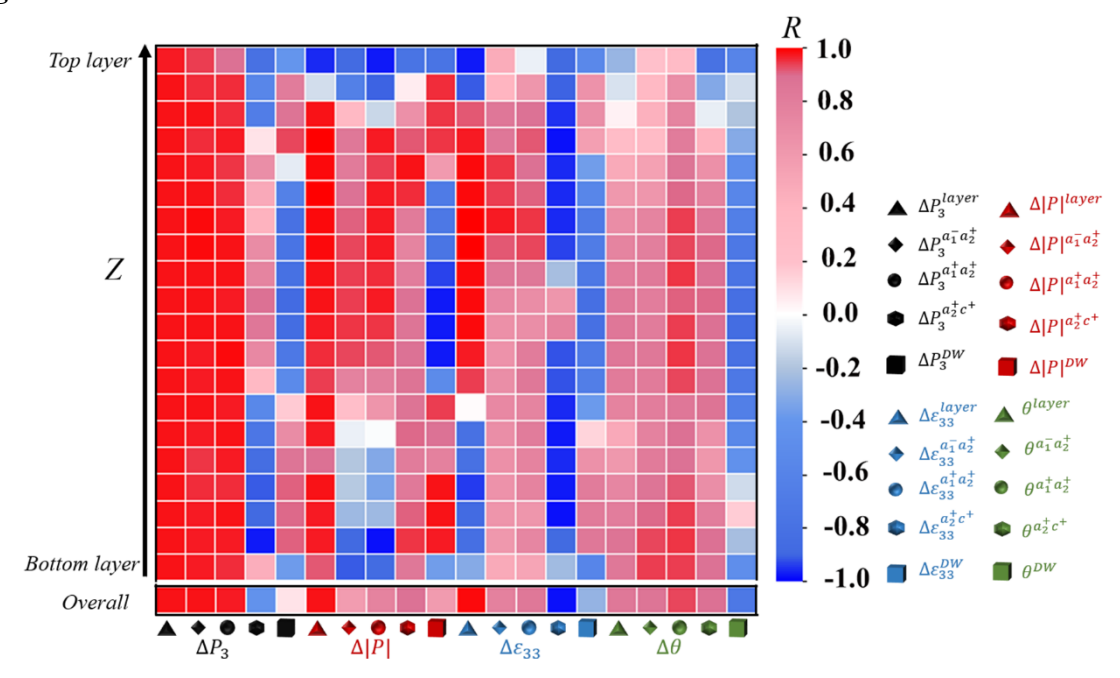


Fig.7 | The correlation between piezoelectric coefficient  $d_{33}^*$  and the variations of out-of-plane strain  $\Delta \varepsilon_{33}$ , out-of-plane polarization  $\Delta P_3$ , the polarization modulus |P| and rotation angle  $\theta$ , with each annotated in black, red, blue and green colors. For the correlation of each factor, the average of entire layer,  $a_1^-a_2^+$  domain,  $a_1^+a_2^+$  domain and  $a_2^+c^+$  domain and domain wall are represented by triangle, diamond, circle, hexagon and square symbols, respectively.

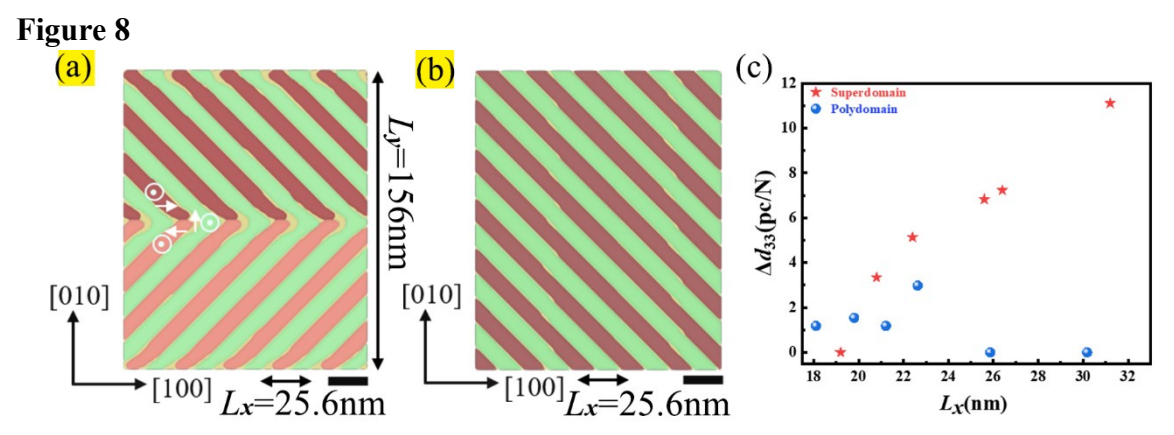


Fig.8 | Tuning the domain size effect on piezoelectricity of the  $a_1c/a_2c$ -type superdomains. (a) Schematic representation of the stripe-like superdomains and polydomain. The in-plane misfit strain is  $\varepsilon_{11}^{mis} = \varepsilon_{22}^{mis} = 0.075\%$ , and the temperature is 400 K. (b) The variation of the out-of-plane piezoelectric coefficient  $\Delta d_{33}^*$  as a function of  $L_x$ .

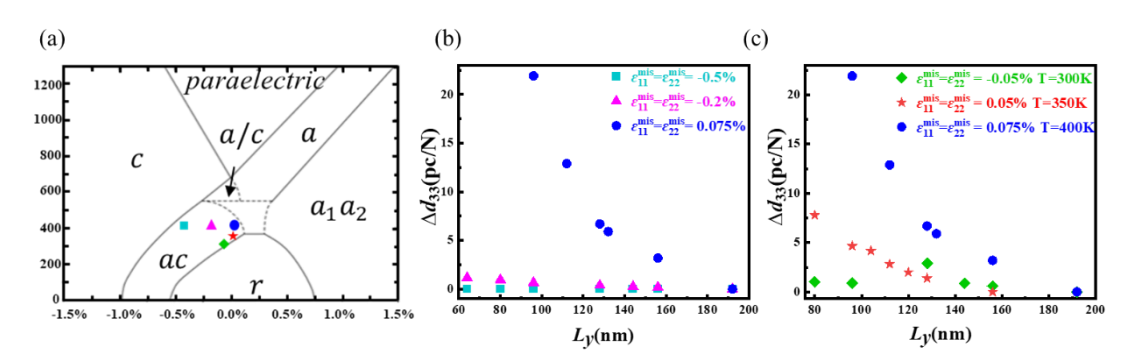


Fig.9 | Tuning the domain size effect on piezoelectricity of the  $a_1c/a_2c$ -type superdomains. (a) Temperature-misfit strain phase diagrams of  $K_{0.5}Na_{0.5}NbO_3$ . The meaning of symbols for domain variants are:  $a(P_1 \neq 0, P_2 = P_3 = 0 \text{ or } P_2 \neq 0, P_1 = P_3 = 0), c(P_3 \neq 0, P_1 = P_2 = 0), ac (P_1 \neq 0, P_2 = 0, P_3 \neq 0 \text{ or } P_1 = 0, P_2 \neq 0, P_3 \neq 0), a_1a_2(P_1 \neq 0, P_2 \neq 0, P_3 = 0), r (P_1 \neq 0, P_2 \neq 0, P_3 \neq 0))$ . (b-c) The variation of the out-of-plane piezoelectric coefficient  $\Delta d_{33}^*$  as a function of  $L_x$  for stripe-like superdomains (b) under various in-plane misfit strains of  $\varepsilon_{11}^{mis} = \varepsilon_{22}^{mis}$  at 400 K and (c) under varied misfit strains and temperatures. (a) is reprinted with adaption from Ref. [43]. With the permission of AIP Publishing.

## **Supporting Figure 1**

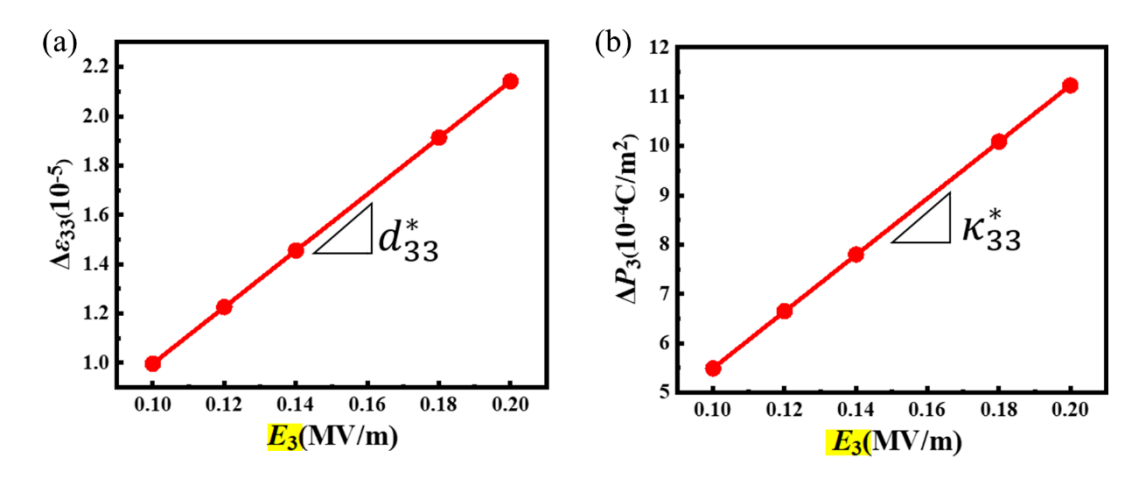


Fig.S1 | Example of the evaluation of the out-of-plane piezoelectric coefficient in the phase-field simulation. (a) The variation of out-of-plane strain  $\Delta \varepsilon_{33}$  as a function of the applied electric field  $E_3$ . The slope of a linear fitting line gives the  $d_{33}^*$ . (a) The variation of the out-of-plane polarization  $\Delta P_3$  as a function of the applied electric field  $E_3$ . The slope of a linear fitting line gives the  $\kappa_{33}^*$ .

## **Supporting Figure 2**

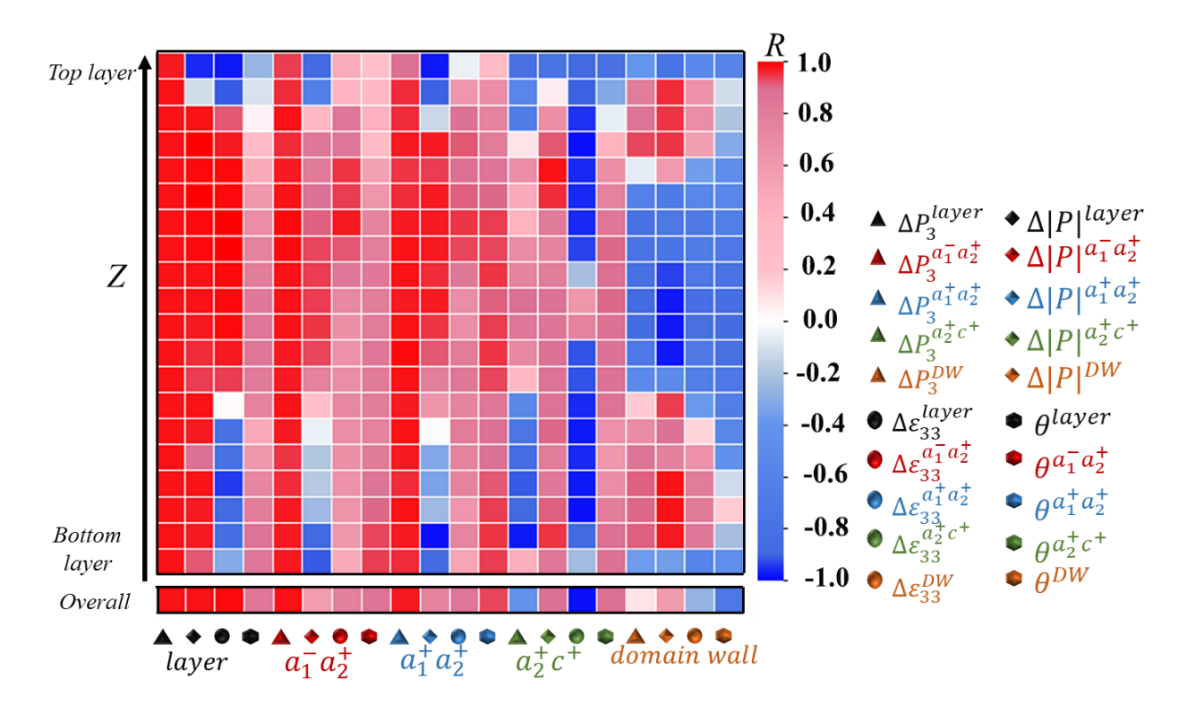


Fig. S2 | The replotting of Fig.7 by reorganizing the columns of the R matrix in terms of the types of domain variants and domain walls.

## **Supporting Figure 3**

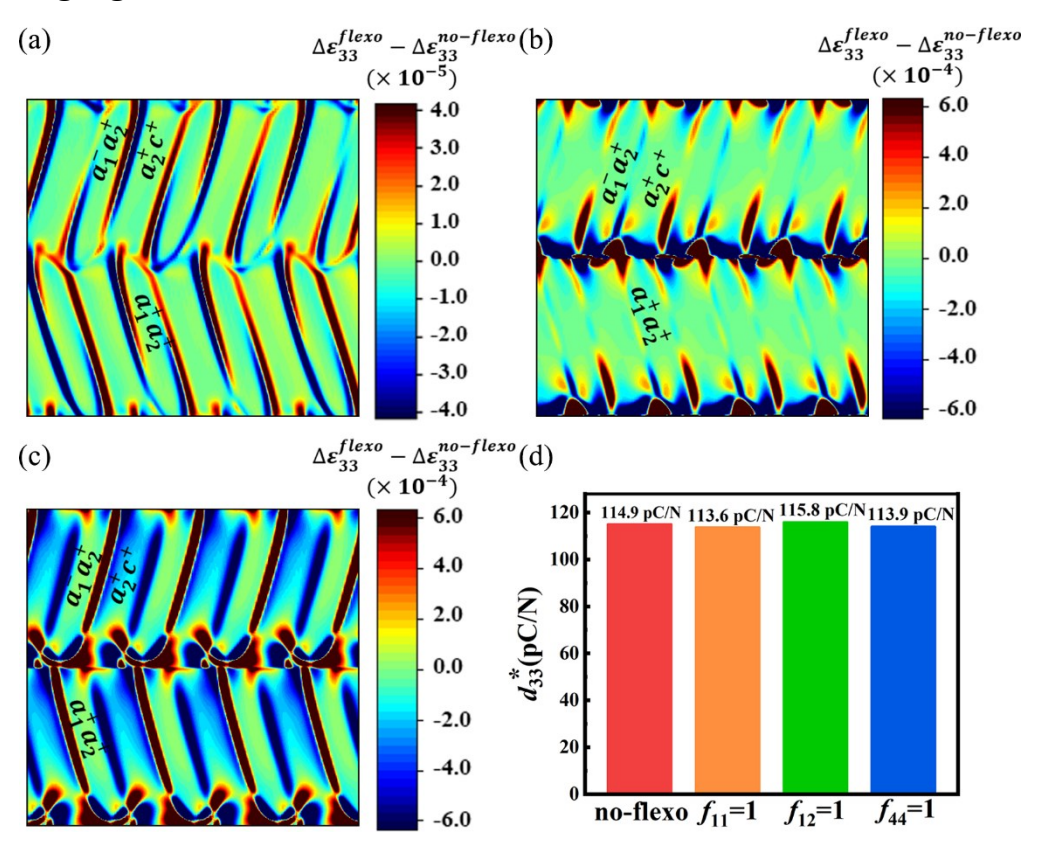


Fig.S3 | The influence of flexoelectric effect on piezoelectric response. (a-c) The mapping of  $\Delta \varepsilon_{33}^{\text{flexo}} - \Delta \varepsilon_{33}^{\text{no-flexo}}$  for the middle layer of KNN thin film considering flexoelectric coefficients of (a)  $f_{11}$ =1 V,  $f_{12}$ =0,  $f_{44}$ =0, (b)  $f_{11}$ =0,  $f_{12}$ =1 V,  $f_{44}$ =0, and (c)  $f_{11}$ =0,  $f_{12}$ =0,  $f_{44}$ =1 V. (d) The calculated overall out-of-plane piezoelectric coefficient  $d_{33}^*$  with and without flexoelectric effect.